Volume 13
Number 36
28 September 2025
Pages 11091–11474

Journal of Materials Chemistry B

Materials for biology and medicine

rsc.li/materials-b

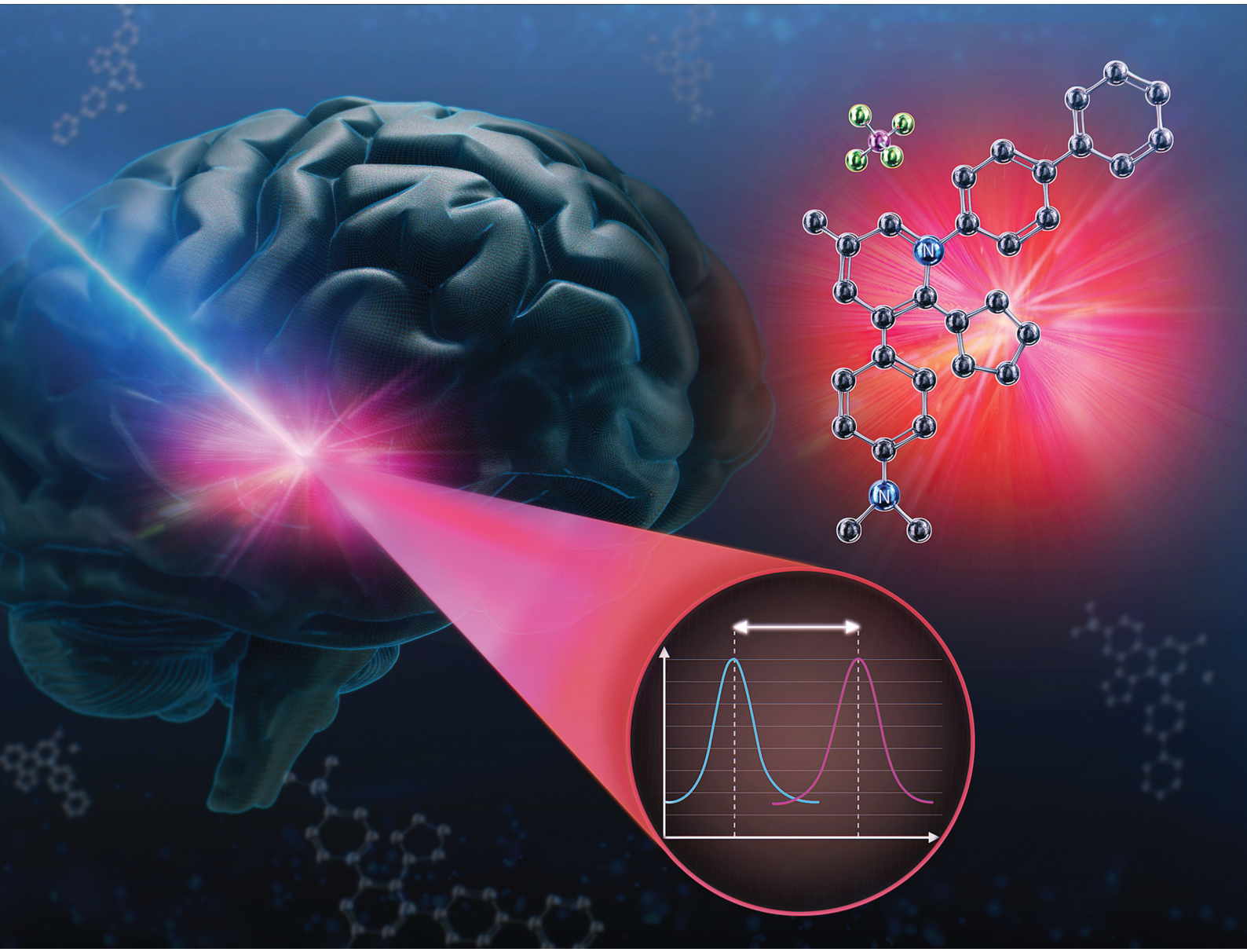

ISSN 2050-750X

ROYAL SOCIETY OF CHEMISTRY

PAPER

Jung Yeol Lee, Beomsue Kim *et al.*
Discovery of asymmetric pyridinium-based fluorescent probes with large Stokes shifts for live neural stem/progenitor cells

Journal of Materials Chemistry B

ROYAL SOCIETY OF CHEMISTRY

PAPER

View Article Online
View Journal | View Issue

Cite this: J. Mater. Chem. B, 2025, 13, 11224

Discovery of asymmetric pyridinium-based fluorescent probes with large Stokes shifts for live neural stem/progenitor cells

Ye Ri Han, †[a] Dongwan Ko, †[b] Yeongran Hwang, [b] Myeong A Choi,[c] Do-Geun Kim,[d] Jung Yeol Lee*[c] and Beomsue Kim *[b]

Received 12th April 2025,
Accepted 23rd July 2025

DOI: 10.1039/d5tb00857c

rsc.li/materials-b

Fluorescent dyes are widely used in biological systems, yet the number of fluorescent scaffolds with desirable photophysical properties remains limited. Herein, we report the synthesis of novel asymmetric pyridinium salts *via* facile Rh(III) C–H activation. A structure–activity relationship (SAR) study led to the identification of a lead candidate, **KD01**, which exhibits a large Stokes shift (Ex/Em = 405/605 nm) and bright fluorescence only upon interaction with live brain cells. Remarkably, **KD01** selectively labels undifferentiated human neural stem/progenitor cells (NSPCs) over differentiated neural cells. This selectivity is likely due to the probe's interaction with the unique biochemical or physical properties of the NSPC cytoplasm, such as binding to an abundant biomolecule. This work presents a bioactive fluorescent scaffold with unique optical properties and NSPC selectivity, offering a promising platform for live-cell imaging and targeted neural cell identification.

Introduction

Although the use of fluorescent organic molecules in biological applications has gradually increased, most of them still rely on a few fluorescent cores to generate their fluorescence, such as xanthene, cyanine, coumarin, and BODIPY.[1–5] While chemical modifications such as antibody conjugation or the attachment of functional motifs *via* linkers have extended their utility, recent strategies have also focused on introducing minimal chemical motifs directly onto the fluorophore backbone to expect specific biological functions.[6,7] However, these modified derivatives are predominantly derived from a limited set of well-established fluorophores and thus retain similar photophysical properties to their parent structures. Recent efforts have been directed toward expanding the repertoire of fluorogenic probes beyond conventional scaffolds. For instance, structurally novel fluorophores with enhanced environment-responsive fluorescence or aggregation-induced emission have been developed, offering improved photophysical diversity and applicability to live-cell or tissue imaging.[8–11] The development of new, atypical fluorescent scaffolds is expected to yield fluorophores with unique photophysical properties, wherein even minor structural modifications could result in significant optical changes.

Among the recently proposed structures for small fluorescent probes, pyridinium salts have attracted great attention due to their versatile properties, including applications as dyes, pharmaceuticals, ionic liquids, phase-transfer agents, and molecular sensors.[12–18] They also serve as key intermediates in natural compounds that contain pyridine, hydropyridine and piperidine moieties.[19–27] Recent studies have demonstrated that pyridinium salts can be synthesized in moderate to high yield *via* transition metal-catalyzed C–H activation.[28,29] This highly efficient reaction strategy enables facile functionalization of the pyridinium salt core by introducing various functional groups, enabling full-color-tunable fluorescence spectra through intracellular charge transfer (ICT).[29,30]

Applying asymmetry to a known fluorescent scaffold can substantially improve its performance in biological contexts. This structural modification enhances molecular compatibility with complex biomolecular surfaces, increases binding specificity, and enables the spatial separation of recognition and signalling domains. Moreover, the induced electronic asymmetry further facilitates ICT, yielding large Stokes shifts and reducing background interference in biologically complex environments.[33]

[a] Department of Chemistry, Duksung Women's University, Seoul 01369, Republic of Korea
[b] Neural Circuit Research Group, Korea Brain Research Institute, 61, Cheomdan-ro, Dong-gu, Daegu, Republic of Korea. E-mail: kimbs@kbri.re.kr
[c] New Drug Development Center, Daegu-Gyeongbuk Medical Innovation Foundation, 80 Chembok-ro, Dong-gu, Daegu, Republic of Korea. E-mail: leejysg@kmedihub.re.kr
[d] Dementia Research Group, Korea Brain Research Institute, 61, Cheomdan-ro, Dong-gu, Daegu, Republic of Korea
† These authors contributed equally.

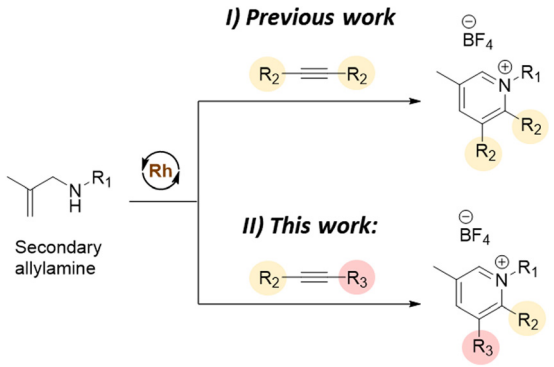

Fig. 1 Synthesis of novel asymmetric pyridinium salts by Rh(III)-catalyzed C–H activation using asymmetric internal alkyne and secondary allylamine.

In this study, we employed an advanced synthetic strategy using asymmetric alkynes to design small, biologically active fluorescent pyridinium salts, aiming for selective activity toward specific live brain cells (Fig. 1). These fluorescent dyes were synthesized *via* a facile, one-step Rh(III)-catalyzed *N*-annulation method. By introducing conjugation to retain desirable wavelengths in asymmetric pyridinium salts for bio-imaging, we identified several hit compounds that exhibited fluorescence exclusively upon application in live cell imaging.

Experimental section

General

^{1}H nuclear magnetic resonance (NMR) and ^{13}C NMR spectra were recorded on an Avance II/DPX 400 (400 MHz ^{1}H, 100 MHz ^{13}C) spectrometer (Bruker, Billerica, MA, USA) with chemical shifts reported relative to residual deuterated solvent peaks. The ^{1}H NMR spectra are reported as follows: chemical shift and multiplicity (s = singlet, d = doublet, t = triplet, q = quartet, m = multiplet, dd = doublet of doublet, and ddd = doublet of doublet of doublet). The ^{13}C NMR spectra were referenced to the residual $CDCl_3$ (77.26 ppm) and MeOD-d_4 (47.59 ppm). The final compounds were purified by preparative high-performance liquid chromatography (HPLC) on a Kinetex 5 mm biphenyl 100 Å GX-281 HPLC system (Gilson, Middleton, WI, USA; column tube 250 × 21.2 mm inner diameter), with ACN/H_2O as the eluent.

Photophysical properties

The absorption coefficient was measured using the Beer–Lambert law. $A = \varepsilon CL$, where A is the absorbance, ε is the absorption coefficient (M^{-1} cm^{-1}), C is the concentration (M), and L is the path length (cm). The concentration of the compound is made up to 1 mM and dispensed into a 96-well plate (100 μL has a path length of 0.29 cm, reference), and the absorbance at 400 nm is measured using Spectramax.

The fluorescence quantum yield (Φ) was determined using a comparative method with a standard fluorophore.[7] Briefly, solutions of the sample (x) and standard (st) were prepared. The absorbance of each solution (A_x and A_{st}) was measured at the same excitation wavelength. The integrated fluorescence intensity (F) was then obtained from the emission spectra, and the QY was calculated according to the following equation, using the refractive index (η) of the respective solvents:

$$\Phi_x = \Phi_{st} \times (A_{st}/A_x) \times (F_x/F_{st}) \times (\eta_x^2/\eta_{st}^2)$$

Cell culture

All culture media were purchased from Invitrogen (USA), unless otherwise specified. SH-SY5Y, a human neuroblastoma cell line, was obtained from ATCC (USA) and maintained under the standard culture medium (DMEM supplemented with 10% (v/v) FBS, 2 mM L-glutamine, 100 U per mL penicillin, and 100 μg per mL streptomycin). To induce differentiation, the medium was replaced with Stage I medium (DMEM supplemented with 2.5% (v/v) FBS, 10 μM retinoic acid, 2 mM glutamine, 100 U per mL penicillin, and 100 μg per mL streptomycin) and cells were cultured for five days. Subsequently, the medium was changed to Stage II medium (neurobasal medium supplemented with 2% B27, 1% GlutaMAX, 10 μM retinoic acid, 50 ng per mL BDNF, 100 U per mL penicillin, and 100 μg per mL streptomycin) for additional five days.[31–33]

ReNcell VM (SCC008), a human neural progenitor/stem cell line, was obtained from Merk (USA) and cultured in ReNcell maintenance medium (neurobasal medium supplemented with 2% B27, 1% GlutaMAX, 20 ng per mL EGF, 20 ng per mL bFGF, 100 U per mL penicillin, and 100 μg per mL streptomycin). Before seeding, culture plates were coated with laminin (20 μg per mL in DMEM/F12) for 4 hours at 37 °C, and incubated in a 5% CO_2 incubator. After incubation, the laminin solution was aspirated, and the plates were rinsed once with PBS. ReNcell cultures were maintained by replacing the medium with fresh ReNcell maintenance medium every other day. To induce differentiation, the medium was replaced with ReNcell maintenance medium lacking EGF and bFGF, and cells were cultured for two weeks with medium changes every 2–3 days.[34]

Epi-fluorescence microscopy

SH-SY5Y cells were incubated with 10 μM of the fluorescent compound and a 650 nm red nuclear dye (Bio tracker 650 red nuclear dye, Sigma-Aldrich, SCT119, 1/1000, USA) in standard culture medium at 37 °C in a 5% CO_2 incubator for 1 hour. Live-cell fluorescence imaging was performed using a Nikon A1Rsi confocal microscope with a 32-channel spectral detector. Emission was recorded from 435 nm to 745 nm under 405 nm excitation, at 10 nm intervals.

Immunocytochemistry

Primary neuron and mixed glia cultures labelled with the fluorescent compound, as well as SH-SY5Y cells treated with 10 μM **KD01** for 1 hour and subsequently differentiated for 14 days, were fixed with 4% paraformaldehyde for 20 minutes at room temperature. The fixed cells were permeabilized in PBS-T (0.1% Triton X-100 in PBS) and blocked with 1% BSA-containing PBS-T for 30 minutes. The cells were incubated

overnight at 4 °C with primary antibodies against Tuj-1 (rabbit anti-Tuj-1 antibody, Sigma-Aldrich, T2200, 1/200, USA), ALDH1L1 (rabbit anti-ALDH1L1 antibody, Abcam, ab190298, 1/100, USA), Olig2 (rabbit anti-Olig2 antibody, Abcam, ab109186, 1/100, USA), and Iba-1 (rabbit anti-Iba-1 antibody, Wako, 019-19741, 1/500, Japan). After three washes with PBS, the cells were incubated with fluorescence-conjugated secondary antibodies for 1 hour. Fluorescence images of the labelled cells were acquired using the Nikon A1Rsi confocal microscope. To quantify the co-localization of **KD01** with cell-type specific markers, the total number of cells in each image was first determined by nuclear counterstaining. Within this population, **KD01**-positive cells were then assessed for the presence or absence of signal from lineage-specific markers (Tuj-1, ALDH1L1, Olig2, or Iba-1). The number of cells in each category was quantified using the Cell Counter plugin in ImageJ (NIH).

Flow cytometry

Mouse brains at postnatal day 1 were isolated from female C57BL/6 mice, homogenized using a Pasteur pipette and treated with asymmetric fluorescent pyridinium salts (**6a** to **6m**) (10 μM) in standard culture medium at 37 °C, in a 5% CO_2 incubator for 1 hour.

Wild-type/differentiated SH-SY5Y and ReNcell cells were dissociated into single-cell suspensions using a 60 μm strainer and incubated with **KD01** (10 μM) under the same conditions (37 °C, 5% CO_2, 1 hour in standard culture medium).

Initial gating was created with FSC-A and SSC-A parameters to exclude cell debris. Live singlet cells were subsequently gated using SSC-A and SSC-H parameters. Flow cytometry was conducted using an Attune NxT Analyzer (ThermoFisher Scientific, USA), and fluorescence data of each cell were analyzed using Flowjo software.

All animal procedures were approved by the Institutional Animal Care and Use Committee (IACUC) of Korea Brain Research Institute (KBRI) under protocol ID IACUC-23-00054. C57BL/6N mice aged six to ten weeks were used as source animals.

Results and discussion

Synthesis of asymmetric fluorescent pyridinium salts

In this study, pyridinium salt derivatives were synthesized *via* a Rh(III)-catalyzed one-step *N*-annulation method. The standard procedure employed secondary allylamine (**1**), an asymmetric internal alkyne (**2**), and $NaBF_4$ (**3a**), in the presence of $[Cp^*RhCl_2]_2$ (**4a**) and $Cu(OAc)_2$ (**5a**) in MeOH. The resulting pyridinium salts, prepared as pairs of constitutional isomers (compounds **6** and **6′**, collectively referred to as **Cpd**), were individually purified by preparative HPLC. A total of 23 compounds were obtained and assessed for their fluorescence efficiency. The compounds are summarized in Table S1, and the representative structure was further characterized using ^1H and ^{13}C NMR spectroscopy. Additional derivatives synthesized to explore the substrate scope are listed in Tables S2 and S3, based on their shared core structures. All compounds (**6a–6m**) were systematically analyzed according to three functionalized positions—R^1, R^2, and R^3—within a unified structural framework for comparison (Table 1). The structures and yields of all synthesized compounds are detailed in Tables S1–S3, and complete characterization data are provided in Table S4 and Fig. S1–S3.

Screening the asymmetric pyridinium salts for labelling live brain cells

To explore the potential of asymmetric pyridinium salts for live brain cell labelling, we analyzed their photophysical properties in the polar organic solvent DMSO, a standard medium for *in vitro* screening of fluorescent compounds due to its high solubility and polarity. Surprisingly, all newly synthesized compounds (**6a–6m**) exhibited low quantum yields and absorption coefficients under these conditions (Table 1). Nonetheless, we hypothesized that our pyridinium salts might retain or even enhance their fluorescence after reacting with biomolecules in live cells, considering the substantial differences in fluorescence behavior between organic solvents and the water-, protein-, and lipid-rich cellular environment.[6]

To test this hypothesis, we conducted a fluorescence-based compounds screening assay by incubating each compound with a heterogeneous cell population isolated from the postnatal day 1 mouse brain. The use of Attune NxT flow cytometry with four lasers and multiple bandwidth detection channels enabled us to comprehensively profile the fluorescence properties of the compounds. Notably, eight out of twenty-three compounds started to emit fluorescence upon interaction with brain cells (Table 1). The strongest fluorescence signal was consistently detected in the 405 nm excitation/over 600 nm emission channel, suggesting that these compounds exhibit a large Stokes shift only when exposed to a cellular environment (Fig. S2).

Based on fluorescence intensity relative to untreated controls, we classified the compounds into three response categories: no fluorescence (<5%), weak fluorescence (5–20%), and strong fluorescence (>20%). This classification enabled us to identify promising candidates for further development as brain cell–targeting fluorescent probes.

To clarify the role of individual substituents in the R^1–R^3 position, we compared three representative compounds—**6f′**, **6b**, and **6f** (Fig. 2A). Despite their similarity, they showed distinct fluorescence behaviors depending on the position of each substituent, especially for the dimethylaminophenyl group. Notably, placing the dimethylaminophenyl group at the R^2-position resulted in no fluorescence (*e.g.*, **6f′**), whereas its placement at the R^3-position produced fluorescence (*e.g.*, **6f**) (Fig. 2A).

In accordance with the interpretation, we found that eight compounds (**6b**, **6c**, **6d**, **6e″**, **6f**, **6g**, **6g″**, and **6k**) exhibiting fluorescence in flow cytometry commonly shared a dimethylaminophenyl group at the R^3 position of the pyridinium core, suggesting that this structural element is essential for fluorescence enhancement in live cells (Table 1). However, their

Table 1 Structural analysis of asymmetric pyridinium salts (**Cpd**, **6** and **6′**)[a]

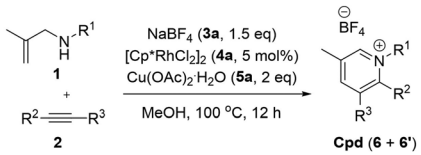

Name	R^1	R^2	R^3	DMSO Quantum yield	DMSO Absorption coefficient (M^{-1} cm^{-1})	Brain cells Fluorescence positive cells (%)
6a	*p*-C_6H_4Ph	Cyclohexyl	*p*-NH_2-C_6H_5	0.005	471.03	3
6b	Ph	cyclopropyl	*p*-$N(CH_3)_2C_6H_5$	0.005	423.79	6.3
6b′	Ph	*p*-$N(CH_3)_2C_6H_5$	Cyclopropyl	0.004	675.86	0
6c (**KD01**)	*p*-C_6H_4Ph	Cyclopentyl	*p*-$N(CH_3)_2C_6H_5$	0.006	448.96	77
6d	CH_2CH_2Ph	Cyclopropyl	*p*-$N(CH_3)_2C_6H_5$	0.005	483.79	6
6d′	CH_2CH_2Ph	*p*-$N(CH_3)_2C_6H_5$	Cyclopropyl	0.004	518.27	0
6e″	*p*-$N(CH_3)_2Ph$	$CH_2CH_2CH_3$	*p*-$N(CH_3)_2C_6H_5$	0.005	528.27	12.5
6f	*p*-C_6H_4Ph	Cyclopropyl	*p*-$N(CH_3)_2C_6H_5$	0.006	462.41	62.3
6f′	*p*-C_6H_4Ph	*p*-$N(CH_3)_2C_6H_5$	Cyclopropyl	0.002	947.93	0
6g	*p*-*N*-Methylpiperazine-Ph	Cyclopropyl	*p*-$N(CH_3)_2C_6H_5$	0.005	547.58	13.9
6g′	*p*-*N*-Methylpiperazine-Ph	*p*-$N(CH_3)_2C_6H_5$	Cyclopropyl	0.003	977.24	0
6g″	*p*-*N*-Methylpiperazine-Ph	$CH_2CH_2CH_3$	*p*-$N(CH_3)_2C_6H_5$	0.005	500.68	13.9
6h	*p*-C_6H_4Ph	Cyclopropyl	3,4,5-Trimethoxyphenyl	0.005	433.44	0
6h′	*p*-C_6H_4Ph	3,4,5-Trimethoxyphenyl	Cyclopropyl	0.007	390.68	0
6i	*p*-C_6H_4Ph	Cyclopropyl	*p*-OMe-C_6H_5	0.037	400.68	0
6i′	*p*-C_6H_4Ph	*p*-OMe-C_6H_5	Cyclopropyl	0.013	375.51	0
6j	*p*-C_6H_4Ph	Cyclopropyl	*p*-CF_3-C_6H_5	0.009	308.62	0
6j′	*p*-C_6H_4Ph	*p*-CF_3-C_6H_5	Cyclopropyl	0.008	298.62	0
6k	*p*-C_6H_4Ph	Cyclohexyl	*p*-$N(CH_3)_2C_6H_5$	0.006	372.06	62.6
6l	*p*-C_6H_4Ph	Cyclopropyl	*m*-OMe, *p*-hydroxy-C_6H_5	0.005	453.79	0
6l′	*p*-C_6H_4Ph	*m*-OMe, *p*-hydroxy-C_6H_5	Cyclopropyl	0.005	431.03	0
6m	*p*-C_6H_4Ph	Cyclopropyl	*p*-CH_3-C_6H_5	0.009	305.51	0
6m′	*p*-C_6H_4Ph	*p*-CH_3-C_6H_5	Cyclopropyl	0.008	310.68	0

[a] Unless otherwise noted, reactions were carried out with **1** (0.2 mmol), **2** (0.4 mmol), **3a** (0.3 mmol), **4a** (5 mol%), and **5a** (0.4 mmol) in 1 mL of MeOH at 100 °C.

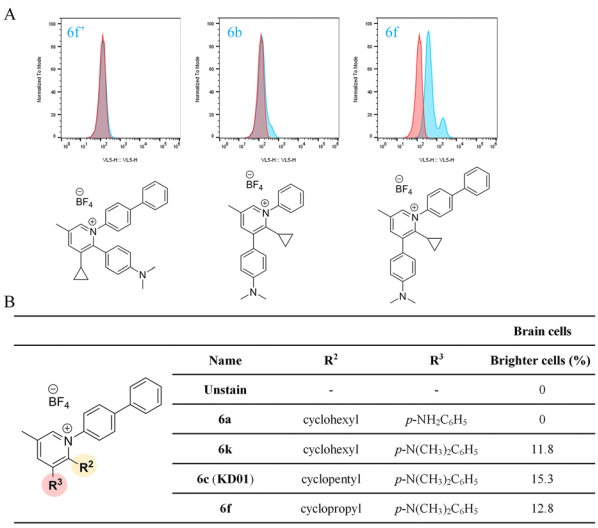

Fig. 2 Structure–activity relationship study of phenyl pyridinium salts. (A) Results of three types of flow cytometry analysis following the treatment of phenyl pyridinium salts in the mouse brain. Cells were incubated with each compound (10 μM) for 1 h at 37 °C in standard culture medium prior to analysis. λ_{Ex} = 405 nm/λ_{Em} = 685–735 nm and (B) identification of structures essential for fluorescence expression through SAR study and comparison of flow cytometry results.

isomer pairs, **6b′**, **6d′**, **6f′** and **6g′**, for **6b**, **6d**, **6f** and **6g**, respectively, showed no fluorescence in live cells (Table 1 and Fig. 2A). Additionally, compound **6a**, which differs from **6k** only by replacing the dimethylaminophenyl group with aminophenyl at the R^3-position, failed to show fluorescence, reinforcing the importance of this motif (Table 1 and Fig. 2B). We next investigated the intensity of the live-cell fluorescence patterns. Among the eight hit compounds, **6c**, **6f**, and **6k** demonstrated particularly strong signals and distinct segregation in flow cytometry plots. These results indicate that they may label specific brain cell types within a heterogeneous population (Fig. 2B). Structural analysis revealed that in the presence of dimethylaminophenyl at R^3, the addition of a biphenyl group at R^1 contributed to the strength of fluorescence and its cell-type specificity (Table 1, **6b** *vs.* **6f** in Fig. 2A), a property not observed in compounds bearing phenyl (**6b**), phenethyl (**6d**) or piperazinylphenyl (**6g**) groups (Table 1). Focusing on the R^2-position, we found that the nature of the cycloalkyl group modulates the fluorescence intensity of labelled brain cells. Among compounds sharing the core structure 1-([1,1′-biphenyl]-4-yl)-3-(4-(dimethylamino)phenyl)-5-methylpyridinium, the cyclopentane-containing compound **6c** showed the strongest fluorescence compared to its cyclopropane (**6k**) and cyclohexane (**6f**) counterparts (Fig. 2B and Fig. S2). Due to its consistent and high fluorescence

intensity as well as distinct cell-type selectivity, we designated **6c** as **KD01** (1-([1,1′-biphenyl]-4-yl)-2-cyclopentyl-3-(4-(dimethylamino)-phenyl)-5-methylpyridin-1-ium tetrafluoroborate), representing the most promising candidate for brain cell-specific fluorescent labelling (Fig. 2B).

Fluorescence specificity of KD01 for neural stem/progenitor cells

From the results of the SAR study, **KD01** was identified, exhibiting strong fluorescence and high clarity in a distinct subpopulation of brain cells. To investigate the specific cell types labelled by **KD01**, we first tested the compound in primary brain cultures, including mixed glial and neuronal cultures. In primary mixed glial cultures, no colocalization was observed between **KD01** fluorescence and established glial cell markers—ALDH1L1 (astrocytes), Olig2 (oligodendrocytes), and Iba-1 (microglia)—indicating that **KD01** does not label these glial subtypes. In contrast, **KD01** selectively labelled a subpopulation of cells in primary mouse neuronal cultures (Fig. 3). Interestingly, **KD01** fluorescence was inversely correlated with Tuj-1 expression, a well-established marker of mature neurons, suggesting that the Tuj-1–negative population may be the primary target of **KD01**.

Since Tuj-1 expression is known to increase with neuronal maturation,[37,38] we hypothesized that **KD01** preferentially stains early-stage neuronal cells.

To verify this, we used the SH-SY5Y human neuroblastoma cell line, which possesses characteristics of neural progenitor cells and can differentiate into mature neuron-like cells upon chemical induction.[41] **KD01** labelling was markedly reduced in differentiated SH-SY5Y cells compared to undifferentiated cells (Fig. 4A, upper panel). During differentiation, **KD01**-positive cells decreased from 99.5% to 22.6%, while **KD01**-negative cells increased from 0.5% to 77.4% (Fig. 4A, lower panel), further supporting the selectivity of **KD01** for undifferentiated neural cell states.

To examine whether **KD01**'s labelling preference extends to *bona fide* neural stem/progenitor cells, we treated ReNcells, a human neural stem/progenitor cell (NSPC) line, with **KD01**. Consistent with SH-SY5Y data, **KD01** fluorescence was prominent in undifferentiated ReNcells (96.3% **KD01**-positive), but significantly reduced upon neural differentiation (18.7% **KD01**-positive; Fig. 4B). These findings indicate that **KD01** preferentially labels NSPC-like populations and loses fluorescence upon neuronal maturation. Additionally, we checked that **KD01** did not affect cell viability or proliferation at the working concentration (10 μM) and did not impair the neuronal differentiation potential of progenitor cells (Fig. S3 and S4).

Consistent with earlier screening results, **KD01** displayed a large Stokes shift across all tested cell types. Spectral confocal fluorescence microscopy confirmed this characteristic: in wild-type ReNcells treated with **KD01** and excited at 405 nm, emission increased up to 605 nm before decreasing toward 745 nm (Fig. 5). Similar emission profiles were observed in undifferentiated SH-SY5Y cells, while differentiated SH-SY5Y cells showed only background-level fluorescence (Fig. 5 and Fig. S5).

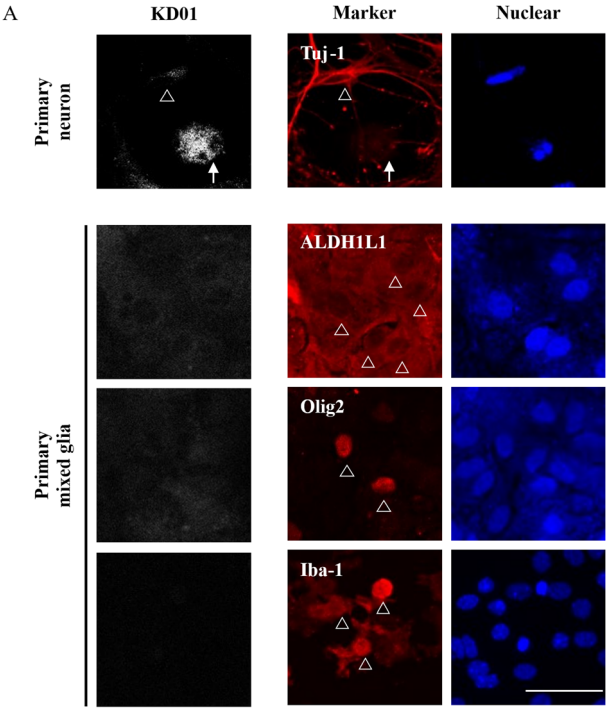

B

Primary neuron	KD01 + / Tuj-1 - 16 / 45
	KD01 + / Tuj-1 + 0 / 22
Primary mixed glia	KD01 + / ALDH1L1 + 0 / 758
	KD01 + / Olig2 + 0 / 82
	KD01 + / Iba-1 + 0 / 256

Fig. 3 **KD01**-mediated fluorescent labelling of primary cultured brain cells. (A) Representative staining pattern of **KD01** in primary neuronal and mixed glial culture. Primary mouse brain cells were incubated with **KD01** (10 μM) for 1 h at 37 °C, followed by fixation and immunostaining with lineage-specific markers: Tuj1 (neurons), ALDH1L1 (astrocytes), Olig2 (oligodendrocytes), and Iba-1 (microglia). DAPI was used for nuclear counterstaining. Arrows indicate **KD01**-positive cells; arrowheads indicate **KD01**-negative cells. (B) Quantification of **KD01**-positive (**KD01**+) cells among the populations positive for brain cell-type markers, as well as Tuj1-negative cells, in both neuronal and glial cultures. Scale bar, 50 μm.

To investigate the mechanism for the selective staining of NSPCs, we hypothesised that **KD01**'s fluorescence is triggered by interaction with specific intracellular components.

We first observed a remarkable fluorescence upon interaction with lysate from SH-SY5Y cells. The fluorescence intensity and pattern of **KD01** incubated with the soluble fraction of the lysate were similar to those observed in intact cells, whereas the insoluble fraction showed a relatively weak signal (Fig. S6). Consistent with these findings, photophysical measurements revealed a synergistic enhancement of its properties: the quantum yield (Φ) increased 5.6-fold (from 0.005 in buffer to 0.028 in lysate), while the molar absorption coefficient (ε) increased over

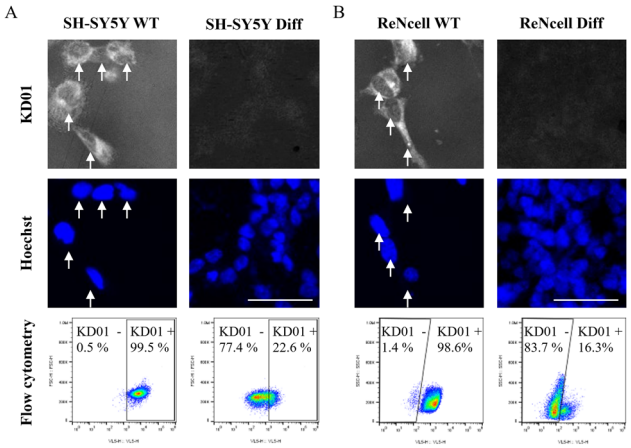

Fig. 4 Specificity of **KD01** for human neural stem/progenitor cells with large Stokes shift fluorescent labelling. (A) Fluorescence images (top) and flow cytometry plots (bottom) of undifferentiated (WT) and differentiated (Diff) SH-SY5Y cells, a human neural progenitor-like cell line. (B) Fluorescence images and flow cytometry plots of ReNcell VM cells, a human neural stem/progenitor cell line. Cells were incubated with **KD01** (10 μM) for 1 h at 37 °C prior to imaging and analysis. Flow cytometry plots were acquired using the 405 nm excitation/685–735 nm emission channel. Scale bar, 50 μm.

A

	KD01 / PBST	KD01 / Cell lysate
QY (ϕ)	0.005	0.028
ε ($M^{-1}cm^{-1}$)	348	4,286

B

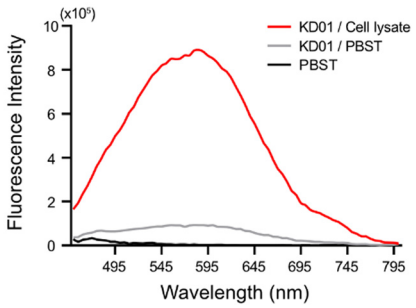

Fig. 6 Photophysical properties of **KD01** in response to cell lysate. (A) Summary of key photophysical properties of **KD01** in lysis buffer and cell lysate. Φ, quantum yield; ε, absorption coefficient. (B) Normalized fluorescence emission spectra of **KD01** (10 μM) in lysis buffer (grey line) and in cell lysate (red line), compared to the buffer blank (PBST, black line). Spectra were recorded with excitation at 405 nm.

12-fold (from 348 to 4286 M^{-1} cm^{-1}) (Fig. 6A). Together, these changes resulted in an approximately 69-fold increase in the overall brightness ($\varepsilon \times \Phi$) of **KD01**, a hallmark of a high-performance fluorogenic probe (Fig. 6B).

This large fluorogenic turn-on response is consistent with established mechanisms where probe fluorescence is activated by interaction with the intracellular environment, such as binding to proteins or sensing viscosity.[35,36] We therefore propose that the selective staining by **KD01** is likely due to either direct binding to an NSPC-abundant biomolecule or a response to the unique physical environment in the NSPC cytoplasm (Fig. 6 and Fig. S6).

The biological significance of NSPCs is well established in both basic neuroscience and translational research, particularly in cell-based therapies for neurodegenerative diseases such as Parkinson's disease, Alzheimer's disease, and amyotrophic lateral sclerosis.[39–41] Transplanted NSPCs can replace damaged neurons, modulate inflammation, promote tissue repair, and support motor function.[42–45] However, the therapeutic success of NSPC transplantation critically depends on the purity of the

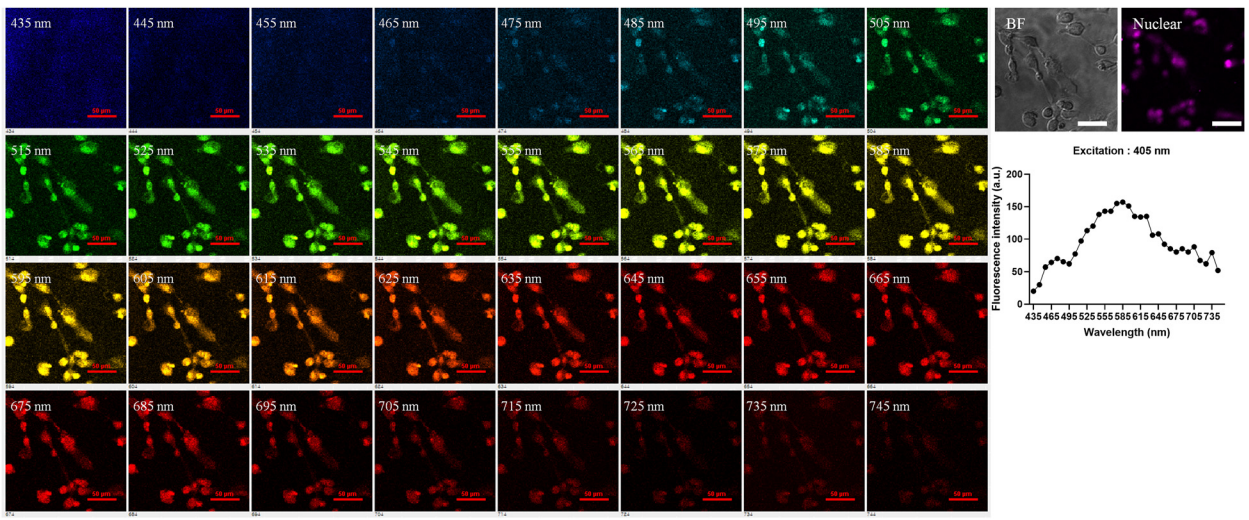

Fig. 5 Spectral confocal microscopy of **KD01**. Representative spectral confocal images of live undifferentiated ReNcells stained with **KD01**. Cells were incubated with **KD01** (10 μM) for 1 h at 37 °C prior to imaging. Fluorescence emission images were captured at 10 nm intervals from 435 to 745 nm following excitation at 405 nm. The fluorescence emission profile of **KD01** from a selected area of interest is shown in the bottom-right panel. BF, bright-field images of the live cells; nuclear, nuclear staining. Scale bar, 50 μM.

cells at specific developmental stages. To achieve this, both improved culture-based enrichment methods and reliable isolation techniques are essential.

KD01 was initially screened in mouse-derived brain cells but exhibited similar performance in human neuronal progenitor/stem cells, suggesting its cross-species applicability as a neural progenitor cell probe.

Our results highlight the potential of **KD01** as a simple, non-invasive, and broadly applicable fluorescent probe to selectively label undifferentiated NSPCs, offering a practical tool for both basic research and clinical applications.

Conclusions

In this study, we developed a novel asymmetric fluorescent pyridinium based bioactive fluorescence scaffold. SAR analysis revealed that specific substitution patterns critically influence fluorescence behavior in live cells. Among the synthesized compounds, **KD01**—bearing a 3-(4-(dimethylamino)phenyl)-5-methylpyridinium motif—demonstrated selective and strong fluorescence labelling, attributed to its large Stokes shift and high compatibility with cellular environments.

KD01 was shown to preferentially stain undifferentiated neural progenitor populations across both mouse- and human-derived cell systems, including primary neuronal cultures, SH-SY5Y cells, and ReNcells. These findings suggest that **KD01** can serve as a valuable tool compound for identifying and tracking NSPCs in heterogeneous cell populations.

Due to its unique chemical structure and live-cell compatibility, **KD01** holds promise as a next-generation brain imaging probe. Further studies should focus on elucidating the molecular mechanism underlying its selective staining and expanding its application to *in vivo* models and clinical-grade stem cell tracking.

Author contributions

The project was conceptualized by B. Kim, J. Y. Lee, and Y. R. Han. B. Kim and J. Y. Lee supervised the project. Y. R. Han synthesized the compounds, and D. Ko performed the biological experiments and photophysical analysis. The manuscript was drafted by Y. R. Han and D. Ko and subsequently revised by Y. R. Han, D. Ko, and B. Kim. Y. Hwang contributed to the initial biological experiments. M. A. Choi assisted with compound synthesis. D.-G. Kim contributed to funding acquisition and project administration. All authors discussed the results and commented on the manuscript.

Conflicts of interest

The authors intend to file a patent application related to the results of this study.

Data availability

The authors confirm that the data supporting the findings of this study are available within the article and its SI. Additional data may be obtained from the corresponding author upon reasonable request.

Additional experimental procedures, supplementary tables and supplementary figures are available. See DOI: **https://doi.org/10.1039/d5tb00857c**

Acknowledgements

This research was supported by the 2021R1C1C1009541 and 2021R1C1C1012378, Korea Drug Development Fund funded by Ministry of Science and ICT, Ministry of Trade, Industry, and Energy, and Ministry of Health and Welfare (RS-2023-00283494). Additionally, it was supported by the National Research Foundation of Korea (NRF) grant funded by the Korea government (MSIT) (RS-2024-00508681), for the establishment of a Korea-UK preclinical/clinical joint research center aimed at developing diagnosis and treatment strategies for neurodegenerative diseases. Furthermore, the work was supported by the KBRI basic research program through the Korea Brain Research Institute, funded by the Ministry of Science and ICT (25-BR-01-03, 25-BR-07-01, and 25-BR-08-01). The Spectramax microplate reader, Nikon A1Rsi confocal microscope, Imaris program, and Attune NxT flow cytometry analyzer were supported by Brain Research Core Facilities in KBRI.

Notes and references

1 M. Moumaris, B. Rajoelya and N. Abuafa, *Open Biol. Sci. J.*, 2015, **1**, 7–15.
2 J. F. Buckman, H. Hernández, G. J. Kress, T. V. Votyakova, S. Pal and I. J. Reynolds, *J. Neurosci. Methods*, 2001, **104**, 165–176.
3 K. Y. Win and S.-S. Feng, *Biomaterials*, 2005, **26**, 2713–2722.
4 L. L. Listenberger and D. A. Brown, *Curr. Protoc. Cell Biol.*, 2007, **35**, 24.22.21.
5 B. Qiu and M. C. Simon, *Bio-protoc.*, 2016, **6**, e1912.
6 B. Kim, M. Fukuda, J. Y. Lee, D. Su, S. Sanu, A. Silvin, A. T. Khoo, T. Kwon, X. Liu and W. Chi, *Angew. Chem.*, 2019, **131**, 8056–8060.
7 J. C. Er, C. Leong, C. L. Teoh, Q. Yuan, P. Merchant, M. Dunn, D. Sulzer, D. Sames, A. Bhinge and D. Kim, *Angew. Chem., Int. Ed.*, 2015, **54**, 2442–2446.
8 D. Si, Q. Li, Y. Bao, J. Zhang and L. Wang, *Angew. Chem., Int. Ed.*, 2023, **62**, e202307641.
9 X. Wang, Q. Ding, R. R. Groleau, L. Wu, Y. Mao, F. Che, O. Kotova, E. M. Scanlan, S. E. Lewis, P. Li, B. Tang, T. D. James and T. Gunnlaugsson, *Chem. Rev.*, 2024, **124**, 7106–7164.
10 S. Munan, Y.-T. Chang and A. Samanta, *Chem. Commun.*, 2024, **60**, 501–521.
11 Y. R. Han and S. B. Lee, *J. Mater. Chem. B*, 2025, **13**, 6044–6060.
12 V. G. Machado, R. I. Stock and C. Reichardt, *Chem. Rev.*, 2014, **114**, 10429–10475.

13 H. Lee, S. J. Moon, Y. D. Yoo, E. J. Jeong and J. R. Rho, *J. Nat. Prod.*, 2022, **85**, 1495–1502.
14 T. Welton, *Chem. Rev.*, 1999, **99**, 2071–2084.
15 A. Hazra, C. Ghosh, F. Banerjee and S. K. Samanta, *ACS Appl. Polym. Mater.*, 2024, **6**, 6540–6551.
16 D. Wu, Y. Yu, J. Zhang, L. Guo and Y. Kong, *ACS Appl. Mater. Interfaces*, 2018, **10**, 23362–23368.
17 J. Yao, Y. Fu, W. Xu, T. Fan, Y. Gao, Q. He, D. Zhu, H. Cao and J. Cheng, *Anal. Chem.*, 2016, **88**, 2497–2501.
18 S. Sowmiah, J. M. S. S. Esperança, L. P. N. Rebelo and C. A. M. Afonso, *Org. Chem. Front.*, 2018, **5**, 453–493.
19 S. Yamada and C. Morita, *J. Am. Chem. Soc.*, 2002, **124**, 8184–8185.
20 J. T. Kuethe and D. L. Comins, *J. Org. Chem.*, 2004, **69**, 5219–5231.
21 D. L. Comins, S. P. Joseph and R. R. Goehring, *J. Am. Chem. Soc.*, 1994, **116**, 4719–4728.
22 C. Legault and A. B. Charette, *J. Am. Chem. Soc.*, 2003, **125**, 6360–6361.
23 C. Y. Legault and A. B. Charette, *J. Am. Chem. Soc.*, 2005, **127**, 8966–8967.
24 M. A. Fernandez-Ibanez, B. Macia, M. G. Pizzuti, A. J. Minnaard and B. L. Feringa, *Angew. Chem., Int. Ed.*, 2009, **48**, 9339–9341.
25 J. A. Bull, J. J. Mousseau, G. Pelletier and A. B. Charette, *Chem. Rev.*, 2012, **112**, 2642–2713.
26 C. Kim, J. Jeong, M. Vellakkaran and S. Hong, *ACS Catal.*, 2022, **12**, 13225–13233.
27 M. Kim, Y. Koo and S. Hong, *Acc. Chem. Res.*, 2022, **55**, 3043–3056.
28 C. Z. Luo, J. Jayakumar, P. Gandeepan, Y. C. Wu and C. H. Cheng, *Org. Lett.*, 2015, **17**, 924–927.
29 Y. R. Han, S. H. Shim, D. S. Kim and C. H. Jun, *Org. Lett.*, 2018, **20**, 264–267.
30 C. Z. Luo, P. Gandeepan, J. Jayakumar, K. Parthasarathy, Y. W. Chang and C. H. Cheng, *Chemistry*, 2013, **19**, 14181–14186.
31 L. Agholme, T. Lindstrom, K. Kagedal, J. Marcusson and M. Hallbeck, *J. Alzheimers Dis.*, 2010, **20**, 1069–1082.
32 J. Kovalevich and D. Langford, *Methods Mol. Biol.*, 2013, **1078**, 9–21.
33 M. M. Shipley, C. A. Mangold and M. L. Szpara, *J. Visualized Exp.*, 2016, 53193.
34 Y. Song, K. Subramanian, M. J. Berberich, S. Rodriguez, I. J. Latorre, C. M. Luria, R. Everley, M. W. Albers, T. J. Mitchison and P. K. Sorger, *Sci. Data*, 2019, **6**, 1–17.
35 S.-W. Yun, C. Leong, D. Zhai, Y. L. Tan, L. Lim, X. Bi, J.-J. Lee, H. J. Kim, N.-Y. Kang, S. H. Ng, L. W. Stanton and Y.-T. Chang, *Proc. Natl. Acad. Sci. U. S. A.*, 2012, **109**, 10214–10217.
36 J. Ma, R. Sun, K. Xia, Q. Xia, Y. Liu and X. Zhang, *Chem. Rev.*, 2024, **124**, 1738–1861.
37 D. Jiang, J. Du, X. Zhang, W. Zhou, L. Zong, C. Dong, K. Chen, Y. Chen, X. Chen and H. Jiang, *Int. J. Mol. Med.*, 2016, **38**, 1367–1376.
38 S. P. Memberg and A. K. Hall, *J. Neurobiol.*, 1995, **27**, 26–43.
39 V. Martinez-Cerdeno and S. C. Noctor, *Front. Neuroanat.*, 2018, **12**, 104.
40 R. M. Seaberg and D. van der Kooy, *Trends Neurosci.*, 2003, **26**, 125–131.
41 C. C. Homem, M. Repic and J. A. Knoblich, *Nat. Rev. Neurosci.*, 2015, **16**, 647–659.
42 M. Aceves, A. Tucker, J. Chen, K. Vo, J. Moses, P. Amar Kumar, H. Thomas, D. Miranda, G. Dampf, V. Dietz, M. Chang, A. Lukose, J. Jang, S. Nadella, T. Gillespie, C. Trevino, A. Buxton, A. L. Pritchard, P. Green, D. A. McCreedy and J. N. Dulin, *Commun. Biol.*, 2023, **6**, 544.
43 I. Fischer, J. N. Dulin and M. A. Lane, *Nat. Rev. Neurosci.*, 2020, **21**, 366–383.
44 D. M. Hermann, L. Peruzzotti-Jametti, J. Schlechter, J. D. Bernstock, T. R. Doeppner and S. Pluchino, *Front. Cell. Neurosci.*, 2014, **8**, 291.
45 H. Suzuki, Y. Imajo, M. Funaba, N. Nishida, T. Sakamoto and T. Sakai, *Front. Cell. Neurosci.*, 2021, **15**, 794692.